J Appl Electrochem (2013) 43:805–815
DOI 10.1007/s10800-013-0565-y

ORIGINAL PAPER

# Effect of titania particles preparation on the properties of Ni–$TiO_2$ electrodeposited composite coatings

**S. T. Aruna · M. Muniprakash · V. K. William Grips**

Received: 7 March 2013 / Accepted: 13 May 2013 / Published online: 25 May 2013


**Abstract** In this paper, the effect of titania particles preparation on the properties of Ni–$TiO_2$ electrocomposite coatings has been addressed. Titania particles were prepared by precipitation method using titanium tetrachloride as the precursor. The titanyl hydroxide precipitate was subjected to two different calcinations temperatures (400 and 900 °C) to obtain anatase and rutile titania particles. These particles along with commercial anatase titania particles were separately dispersed in nickel sulfamate bath and electrodeposited under identical electroplating conditions to obtain composite coatings. The electrodeposited coatings were evaluated for their microhardness, wettability, corrosion resistance, and tribological behavior. The variation of microhardness with current density exhibited a similar trend for all the three composite coatings. The composite coating containing anatase titania particles exhibited higher microhardness and improved wear resistance. However, the corrosion resistance of the composite coating containing commercial titania powder was superior to that of plain nickel, Ni–$TiO_2$ composite coatings containing anatase and rutile titania particles. The poor corrosion resistance of these composite coatings was attributed to the higher surface roughness of the coatings. This problem was alleviated by incorporating ball-milled titania powders. The composite coatings with higher surface roughness were modified with a low surface energy material like fluoroalkyl silane to impart hydrophobic and superhydrophobic properties to the coatings. Among these coatings, Ni–$TiO_2$–9C coating exhibited the highest water contact angle of 157°.

S. T. Aruna (✉) · M. Muniprakash · V. K. William Grips
Surface Engineering Division, Council of Scientific and Industrial Research-National Aerospace Laboratories, Post Bag No. 1779, HAL Airport Road, Bangalore 560 017, India
e-mail: aruna_reddy@nal.res.in

**Keywords** Precipitation · Electrodeposition · Corrosion test · Hardness · Wear

## 1 Introduction

In recent years, there has been a renewed interest in the synthesis and properties of particle reinforced metal matrix nanocomposite coatings, with grain size of both matrix and dispersed particles having less than 100 nm [1]. Such metal matrix nanocomposite coatings are being developed to meet the particular demands of low coefficient of friction and high wear resistance for current advanced technological applications in aerospace, defense, automobile, and nuclear power industries. Several techniques such as electroplating, plasma thermal spray, and physical vapor deposition have been applied to produce protective coatings [2]. Electroplating of composite coating is an effective method to prepare composite coatings through the codeposition of metallic, non metallic or polymer particles with metal and alloys to improve properties such as corrosion resistance, hardness and wear performance [3]. This method has advantages like low cost, low temperature, and single step process without additional thermal treatment [4]. Numerous nickel matrix nanocomposite coatings containing different types of inert nanoparticles such as $TiO_2$, SiC, $CeO_2$, $Al_2O_3$, $Si_3N_4$, $ZrO_2$, carbon nano tubes, diamond, etc., have been electrodeposited from different electrolytes in which the nanoparticles were suspended [5–10].

Titania is the most widely used oxide material after alumina and zirconia because of its good photocatalytic property. It is widely used in self cleaning coatings, pigments, dye-sensitized solar cells etc. Titania exists in three different polymorphs like anatase (5.5–6 Mohs), rutile (6–6.5 Mohs), and brookite (5.5–6 Mohs). Li et al. [11]

prepared Ni–$TiO_2$ composite coating containing sol–gel synthesized $TiO_2$ particles with a maximum hardness value of 7.5 GPa. Yang et al. [12] reported a corrosion resistant Ni–$TiO_2$ composite coating on sintered NdFeB magnet by pulse electrodeposition. Parida et al. [13] reported the application of hexa decylpyridinium bromide to get well-dispersed titania particles in Ni–$TiO_2$ composite coating. Baghery et al. [14] and Sun and Li [15] have also studied the friction and wear properties of electrodeposited Ni–$TiO_2$. Sun and Li [16] reported decreased wear rate and coefficient of friction for Ni–$TiO_2$ coatings with increased titania nanoparticle content. The effects of pulse electrodeposition parameters on the properties of Ni–$TiO_2$ nanocomposite coatings have been reported [17]. Ni–$TiO_2$ coatings were electroplated by the addition of a transparent $TiO_2$ sol into the traditional electroplating Ni solution [18]. In a recent report, Huang and Pan studied the relationship between the microstructure and hydrophobic performance of electrodeposited Ni–$TiO_2$ nanocomposite coatings [19]. In all these studies, Ni–$TiO_2$ electrocomposite coatings were deposited from Ni baths containing commercial titania particles. The comparative properties of Ni–$TiO_2$ electrocomposite coatings containing synthesized and commercial titania powders, have not yet been reported. Either too, there have been no studies on the effect of titania particles preparation on the properties of Ni–$TiO_2$ electrocomposite coatings.

The aims of the present study are as follows: (i) synthesis of anatase and rutile titania particles from the titanyl hydroxide precipitate by calcining the precipitate at two different calcination temperatures; (ii) codeposition of these calcined titania particles in nickel matrix; (iii) evaluation of microhardness, corrosion resistance, wear resistance, and wettability of the composite coatings; and (iv) comparison of the properties of Ni–$TiO_2$ composite coating containing calcined particles with that of the Ni-electrocomposite coating containing titania commercial powder.

## 2 Experimental

### 2.1 Preparation and characterization of $TiO_2$ powders

Titania powders were prepared by a simple chemical precipitation route. Precipitation method is relatively easier and in-expensive method for the preparation of a variety of oxide materials [20]. First, a known amount of titanium tetrachloride (E-Merck) was dissolved in cold dilute 1:1 HCl solution. Then to the obtained $TiOCl_2$ solution, ammonium hydroxide solution (1:1) was slowly added to precipitate out $TiO(OH)_2$ at pH 7. The white precipitate obtained was allowed to settle, filtered, washed with copious amounts of water and dried at 110 °C. The dried powders were calcined at 400 and 900 °C for 4 h and the obtained powders are designated as $TiO_2$–4C and $TiO_2$–9C, respectively. Commercial titania ($TiO_2$–CM–S.D. fine chemicals) powder was used for comparison and the same was also characterized and used for electrodeposition.

The powders were characterized for phase identification and crystallite size using a powder X-ray diffractometer (Bruker D-8 Advanced) with Cu Kα radiation. The morphology of the powders was determined by field emission scanning electron microscopy (FESEM-Carl Zeiss). Raman spectra of the powders were recorded with a DILOR-JOBIN-YVON-SPEX (Paris, France) integrated Raman spectrometer (Model Labram). The particle size distribution of the powders was measured using Mastersizer 2000 particle size analyzer (Malvern instruments).

### 2.2 Preparation of Ni–$TiO_2$ composite coatings

Nickel sulfamate plating bath was prepared by mixing 300 g $L^{-1}$ nickel sulfamate solution (50 g nickel per litre), 10 g $L^{-1}$ nickel chloride, 30 g $L^{-1}$ boric acid and 0.2 g $L^{-1}$ of sodium lauryl sulfate. The Ni-sulfamate plating bath (~200 mL) containing 20 g $TiO_2$ particles (100 g $L^{-1}$) was taken in a glass beaker and stirred overnight. During electrodeposition, the bath was held at room temperature and its pH was maintained at 4 by the addition of sulfamic acid and basic nickel carbonate. A pure nickel sheet (2.5 cm × 12 cm) and a brass substrate with the same dimension were used as anode and cathode, respectively. The polished brass substrate was degreased with acetone followed by cathodic cleaning and acid dipping and finally washed with distilled water. In order to ensure the uniform dispersion of particles, the electrolyte bath containing particles was subjected to magnetic stirring (~600 rpm) for 15 h before the deposition process and also during the electrodeposition. A magnetic stirrer with variable rpm (Remi, India) was used for keeping the particles in suspension. The codeposition was carried out at various current densities using Aplab 7253 regulated DC power supply: 0.23 A $dm^{-2}$ for 20 h, 0.77 A $dm^{-2}$ for 6 h, 1.55 A $dm^{-2}$ for 3 h, 3.1 A $dm^{-2}$ for 1.5 h and 5.4 A $dm^{-2}$ for 45 min, such that the deposit thickness was ~40 μm based on Faraday's laws.

### 2.3 Characterization of Ni–$TiO_2$ composite coatings

#### *2.3.1 XRD, microhardness, and microstructural studies of Ni–$TiO_2$ composite coatings*

The crystalline phases present in the Ni–$TiO_2$ coatings were identified from XRD patterns using JCPDS cards (No. 4-0477 for anatase; 4-055 for rutile and 4-0593 for Ni). The metallographic specimens for cross-sectional studies were

prepared by sandwiching electrodeposited Ni–$TiO_2$ brass coupons with a copper backup in a bakelite matrix followed by mechanical grinding and polishing with $Al_2O_3$ slurry, down to 0.05 μm. The microhardness measurements were performed on ten different locations on the cross-section of each coating (Micromet 2103, Buehler, 50 gf load). The optical micrographs of the cross sections of Ni–$TiO_2$ coatings were recorded using a vertical metallurgical microscope. The area fraction of particles incorporated in the Ni matrix was calculated from the cross-sectional optical micrographs using image analysis software (Videopro 32 supplied by M/s Leading Edge, Australia). The surface morphology of the coatings were observed using FESEM. Surface roughness ($R_a$) of the coatings was measured using a roughness profilometer (Taylor Hobson).

#### 2.3.2 Corrosion studies

The corrosion behavior of Ni and Ni–$TiO_2$ composite coatings electrodeposited at 1.55 A $dm^{-2}$ on mild steel coupons were studied using CHI 604 2D electrochemical workstation. The test was carried out in deaerated 3.5 wt% (0.6 M) NaCl solution (200 ± 2 mL) using conventional three electrode cell equipped with coated brass coupon with an active area of 1 $cm^2$ as working electrode. A platinum foil and saturated calomel electrode were used as counter and reference electrodes, respectively. The reference electrode was connected to a Luggin capillary and its tip was placed very close to the surface of the working electrode to minimize the IR drop. The coupon was immersed in NaCl solution for an hour to establish the open circuit potential ($E_{OCP}$). The EIS studies were carried out in the frequency range of 100 kHz–10 mHz. The amplitude of applied alternating potential was 10 mV on the $E_{OCP}$. The impedance data were displayed as Nyquist and Bode plots, respectively. The Nyquist plot is a plot of real ($Z'$) versus imaginary impedance ($Z''$). The Bode plot is a plot of |Z| versus frequency and frequency versus–phase angle (θ), where |Z| is the absolute impedance. The acquired data were curve fitted and analyzed using ZSimpwin program. After EIS measurements, the system was allowed to attain open circuit potential and then the upper and lower potential limits of linear sweep voltammetry were set at ±200 mV with respect to the EOCP. The sweep rate was 1 mV $s^{-1}$. The Tafel plots obtained have been represented as potential versus log $i$ plot.

#### 2.3.3 Tribological studies

The tribological performance of Ni–titania composite coatings was investigated by conducting wear tests on a pin-on-disk tribometer (DUCOM, India) under the ambient conditions of temperature and humidity (30 °C, 50 % RH) at an applied load of 9.8 N. Wear experiments were undertaken for a minimum of three specimens (in semi-circular brass pins of radius 6 mm) coated with Ni–$TiO_2$ at 1.55 A $dm^{-2}$ for 3 h (~40 μm thickness). All the wear tests were conducted at a wear track radius of 30 mm and 200 rpm (slide speed of 0.628 m $s^{-1}$) to get a constant sliding distance of 4,525 m. Hardened EN 31 steel disk with a Vickers hardness of 750 HV, was used as the counterpart. More details regarding the wear studies have already been reported [21]. The wear coefficient was calculated using the Holm–Archard relationship [22, 23].

#### 2.3.4 Water repellent property of Ni and Ni–$TiO_2$ composite coatings

After electrodeposition, the brass substrates coated with Ni and Ni–$TiO_2$ coatings were rinsed with deionized water, dried and then ethanolic solution of 1 wt% fluoro alkyl silane [FAS-17 (ABCR GmbH)] was sprayed on to the coatings using an ordinary spray gun at room temperature and was allowed to dry at room temperature for 1 h. Then, the substrates were allowed to dry in an oven at 80 °C for 1 h. The water contact angles (WCA) on the surface of Ni and Ni–$TiO_2$ coatings with and without FAS-17 treatment were recorded, using surface electro optics phoenix contact angle meter by sessile drop method at ambient conditions. Water drops (8 μL) were placed on the surface of the coatings and the contact angles were measured. The average value of five measurements at different positions of each coating was adapted as the final WCA.

## 3 Results and discussion

### 3.1 Powder characterization

The powder XRD patterns of titania powders calcined at 400 and 900 °C exhibited pure anatase (JCPDS No. 4-0477) and rutile titania (JCPDS No. 4-055) phases, respectively (Fig. 1a, b). Commercial $TiO_2$ powder also exhibited pure anatase phase (Fig. 1c). From the XRD plots it is clear that $TiO_2$–4C shows XRD line broadening indicating the smaller crystallite sizes compared to $TiO_2$–CM and $TiO_2$–9C powders. The crystallite sizes calculated from XRD line broadening from Scherrer's formula were 16, 103, and 25 nm, respectively for $TiO_2$–4C, $TiO_2$–9C, and $TiO_2$–CM powders, respectively.

Raman spectrum of $TiO_2$–4C shows broad peaks centered around 400 and 500 $cm^{-1}$ corresponding to anatase form of titania (Fig. 2). $TiO_2$–CM powder also showed intense Raman peaks at 400, 515, and 639 $cm^{-1}$ corresponding to anatase phase (Fig. 2). Raman spectrum of $TiO_2$–9C showed strong peaks at 440 and 606 $cm^{-1}$

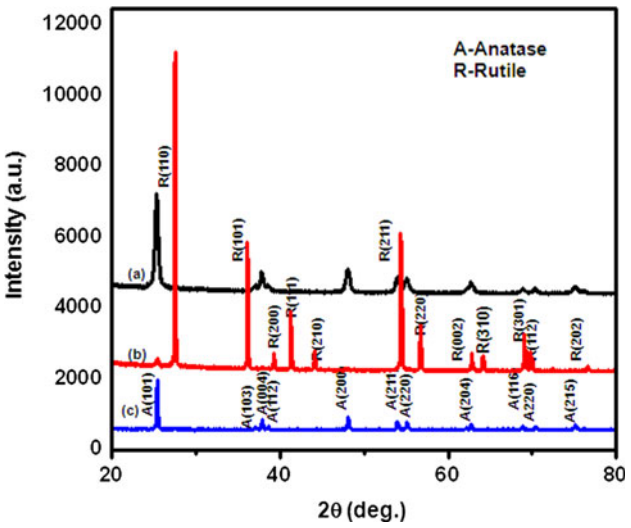


**Fig. 1** Powder XRD patterns of *a* $TiO_2$–4C, *b* $TiO_2$–9C and *c* $TiO_2$–CM (*A* anatase and *R* rutile)

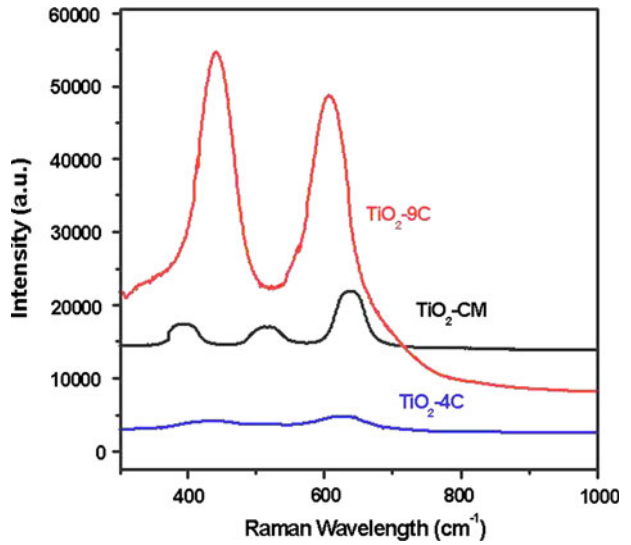


**Fig. 2** Raman spectra of *$TiO_2$–4C*, *$TiO_2$–9C,* and *$TiO_2$–CM* powders

corresponding to pure rutile form of titania (Fig. 2c). The Raman spectral values are in good agreement with the reported values [24].

The FESEM images of titania powders are shown in Fig. 3. The $TiO_2$–4C powders exhibited smaller agglomerated particles, whereas $TiO_2$–9C powders exhibited highly agglomerated, bigger particles. The commercial $TiO_2$ powders exhibited smaller particles with very less agglomeration. The particle size analysis of $TiO_2$–4C powder exhibited a bimodal distribution similar to that of $TiO_2$–CM powder. The average agglomerated particle size of $TiO_2$–4C, $TiO_2$–9C, and $TiO_2$–CM were 1.94, 2.4, and 1.71 μm, respectively. Due to the smaller agglomerated particle size, the commercial powder exhibited better dispersibility in the nickel sulfamate bath. The particle sizes of $TiO_2$–4C and $TiO_2$–9C powders were further reduced by ball milling the powders at 300 rpm for 4 h using planetary monomill (Fritsch) and the obtained powders are designated as $TiO_2$–4C–BM and $TiO_2$–9C–BM. The average agglomerated particle sizes of ball-milled $TiO_2$–4C–BM and $TiO_2$–9C–BM powders were 1.39 and 1.63 μm, respectively.

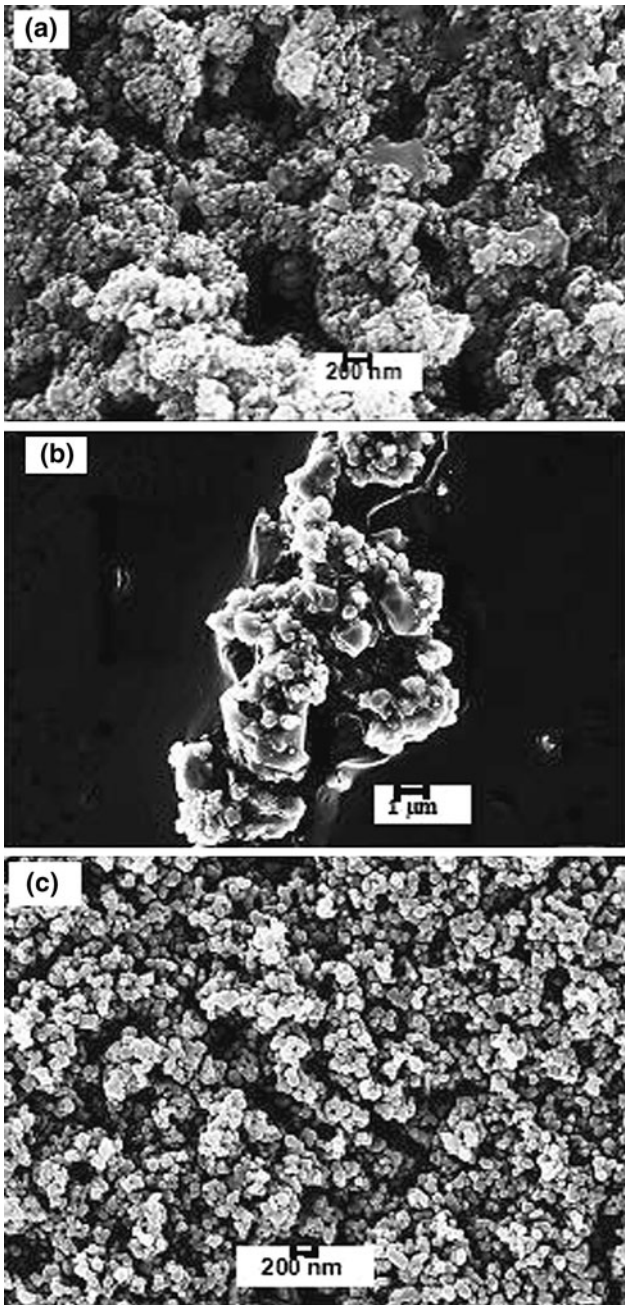


**Fig. 3** FESEM images of powders **a** $TiO_2$–4C, **b** $TiO_2$–9C, and **c** $TiO_2$–CM

### 3.2 Microhardness and microstructure of Ni and Ni–$TiO_2$ composite coatings

The XRD patterns of Ni and Ni–$TiO_2$ composite coatings electrodeposited at 1.55 A $dm^{-2}$ for 3 h are shown in Fig. 4. It can be seen from the XRD patterns that all the coatings viz., Ni, Ni–$TiO_2$–4C, Ni–$TiO_2$–4C–BM, and Ni–$TiO_2$–9C exhibited intense peaks at ~44°, 51°, and 76° corresponding to Ni (111), (200), and (220) planes, respectively. Plain Ni coating exhibited 100 % peak corresponding to Ni(200) and all the Ni–$TiO_2$ composite coatings exhibited the 100 % peak corresponding to Ni(111) orientation. The characteristic peaks of $TiO_2$ anatase and rutile titania were also observed indicating the incorporation of a large fraction of titania particles in the coating (Fig. 4). Also, there was no change in the peak positions or peak widths of the XRD peaks with the incorporation of ball-milled powders.

The plots of Knoops microhardness (50 gF) versus the current density for Ni–$TiO_2$ coatings are shown in Fig. 5. From the plots it is seen that a maximum microhardness of ~580 and 560 HK was obtained for Ni–$TiO_2$–9C and Ni–$TiO_2$–4C, respectively at the lowest current density of 0.77 A $dm^{-2}$. Ni–$TiO_2$–4C and Ni–$TiO_2$–9C show almost similar microhardness values. The increased microhardness has been attributed to the incorporation of large number of titania particles in the Ni-matrix. Similar variations have been reported by Li et al. [11] for Ni–$TiO_2$ nanocomposite coatings containing anatase and rutile titania. The microhardness of Ni–$TiO_2$-commercial coatings was a little lower (~50 HK) than the other two coatings. The plots of microhardness versus current density followed a similar trend having maxima, minima and then maxima for all the three coatings (Fig. 5). At the highest current density used for electrodeposition, all the coatings exhibited similar microhardness values.

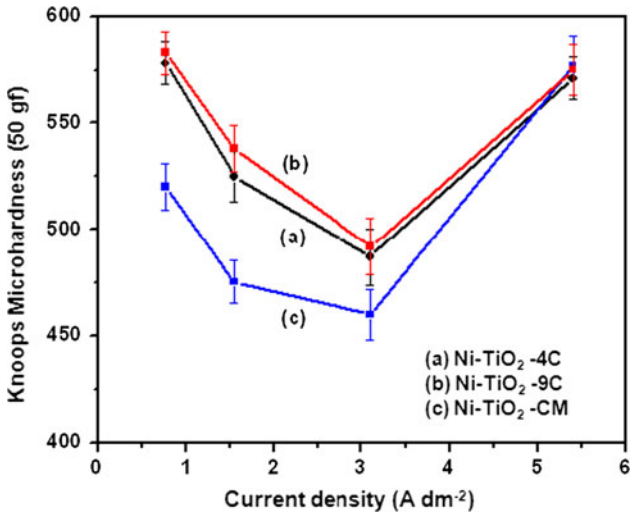


**Fig. 5** Plots of Knoops microhardness vs. applied current density for electrodeposited Ni–$TiO_2$ coatings

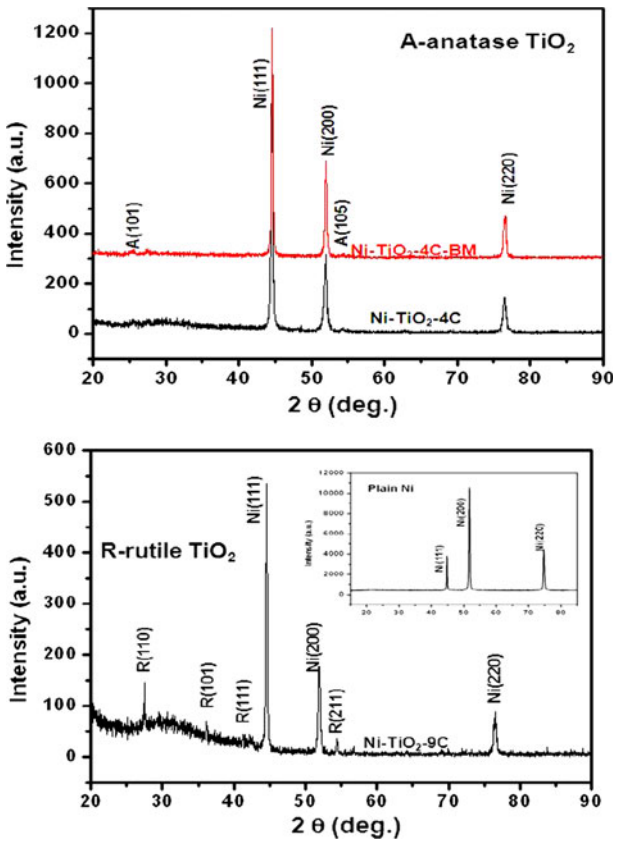


**Fig. 4** XRD patterns of electrodeposited Ni and Ni–$TiO_2$ composite coatings

The cross-sectional optical micrographs of electrodeposited Ni–$TiO_2$ composite coatings are shown in Fig. 6. From the optical micrographs it is evident that Ni–$TiO_2$–CM coating had a larger area fraction of particles and the incorporated particles were more uniformly distributed in the nickel matrix. The area fraction of particles incorporated in the nickel matrix as calculated from optical micrographs were 11–15 %, 8–13 %, and 15–22 %, respectively for Ni–$TiO_2$–4C, Ni–$TiO_2$–9C, and Ni–$TiO_2$–CM coatings electrodeposited at various current densities. For Ni–$TiO_2$–4C and Ni–$TiO_2$–9C coatings electrodeposited at 5.4 A $dm^{-2}$, the area fraction of particles were less and the particles were agglomerated to a larger extent. The large number of particles incorporated in Ni–$TiO_2$–CM coating could be due to the better wettability of commercial powder and also due to the smaller size of the particles. The cross-sectional optical images of Ni–$TiO_2$ composite coatings electrodeposited at 0.55 A $dm^{-2}$ containing ball-milled particles showed uniform distribution of particles with, an area fraction of 19 and 22 % for Ni–$TiO_2$–9C–BM and Ni–$TiO_2$–4C–BM, respectively. Thus by incorporating

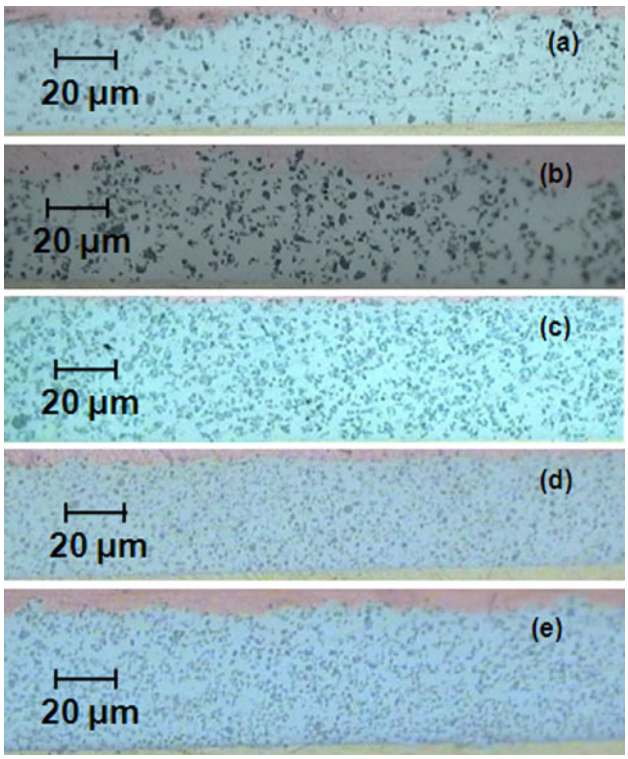


**Fig. 6** Optical micrographs of **a** Ni–$TiO_2$–4C, **b** Ni–$TiO_2$–9C, **c** Ni–$TiO_2$–CM, **d** Ni–$TiO_2$–4C–BM and **e** Ni–$TiO_2$–9C–BM and composite coatings electrodeposited at 0.77 A $dm^{-2}$

ball-milled titania particles, one can achieve particle incorporation equivalent to that of the commercial powder.

The surface topography of electrodeposited Ni–$TiO_2$–4C, Ni–$TiO_2$–4C–BM, Ni–$TiO_2$–9C, and Ni–$TiO_2$–CM coatings are shown in Fig. 7. The microstructure of Ni–$TiO_2$–4C–BM displayed less nodularity and the presence of more titania particles compared to Ni–$TiO_2$–4C (Fig. 7a, b). The surface of Ni–$TiO_2$–9C is very rough containing nodules with titania particles surrounding the nodules (Fig. 7c). The surface of Ni–$TiO_2$–CM coating (Fig. 7d) is smoother and a large number of smaller titania particles are present covering almost the entire coating.

### 3.3 Potentiodynamic polarization and EIS studies of Ni and Ni–$TiO_2$ composite coatings

The potentiodynamic polarization curves obtained for Ni and Ni–$TiO_2$ composite coatings are shown in Fig. 8. The corrosion potential, corrosion current, and the polarization resistance obtained from the Tafel plots are listed in Table 1. When compared to the uncoated substrate, the corrosion potential of the Ni–$TiO_2$–CM coating shifted toward more positive side, indicating the improved corrosion resistance of the coating; while that of Ni–$TiO_2$–4C and Ni–$TiO_2$–9C shifted toward negative side indicating poor corrosion resistance of the composite coatings.

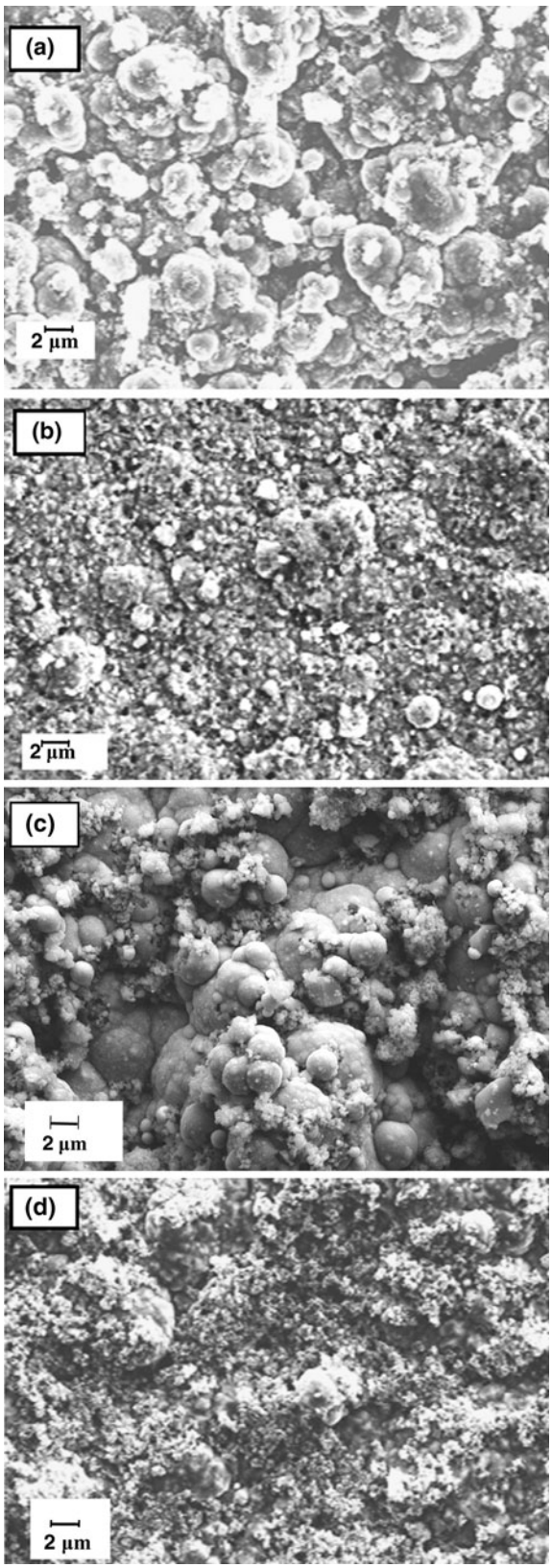


**Fig. 7** FESEM images of electrodeposited **a** Ni–$TiO_2$–4C, **b** Ni–$TiO_2$–4C–BM, **c** Ni–$TiO_2$–9C, and **d** Ni–$TiO_2$–CM composite coatings electrodeposited at 1.55 A $dm^{-2}$

However, the coatings containing ball-milled powders showed improved corrosion resistance compared to Ni–$TiO_2$–CM coating (Fig. 8, inset).

The corrosion current density is an important parameter used for evaluating the kinetics of the corrosion reaction. Corrosion protection is inversely proportional to the corrosion current density. The corrosion current density for the Ni–$TiO_2$–4C–BM coating was very low which also indicates superior corrosion resistance of the coating. The $R_p$ value of Ni–$TiO_2$–4C–BM coating was the highest, implying better corrosion resistance of the coating compared to other coatings.

The Nyquist impedance plots for Ni and Ni–$TiO_2$ coatings are shown in Fig. 9. From the Nyquist plot (Fig. 9) it is evident that the impedance offered by Ni–$TiO_2$–4C–BM and Ni–$TiO_2$–9C–BM coating is higher than Ni, Ni–$TiO_2$–4C, Ni–$TiO_2$–CM, and Ni–$TiO_2$–9C coatings (Fig. 9, inset). In the Nyquist plot, the depressed semicircle with the center under the real axis is characteristic for the solid electrodes. At higher frequencies, interception with the real axis is ascribed to the electrolyte bulk resistance ($R_s$) and at low frequencies an interphase appears whose interception with the real axis is ascribed to the charge transfer resistance ($R_{ct}$). In the Nyquist plot, the diameter of the semicircle corresponding to Ni–$TiO_2$–4C–BM and Ni–$TiO_2$–9C–BM coatings were larger compared to other coatings indicating better corrosion resistance of the coatings. The shape of the impedance spectra describes the type of electrochemical reactions that are taking place on the electrode surface. The impedance plots of Ni and Ni–$TiO_2$ coatings show single time constants behavior. It is concluded that only one mechanism prevailed for the corrosion of the coatings, i.e., nickel dissolution [25].

Bode plots of Ni and Ni–$TiO_2$ composite coatings are shown in Fig. 10. The impedance data obtained from the spectra are tabulated in Table 1. From Table 1, it is evident that $n_{dl}$ value is close to 1 in both Ni and Ni–$TiO_2$–CM coatings indicating more of a capacitive behavior for both the coatings. This is further confirmed by almost similar $Q_{dl}$ values of these coatings. For both Ni–$TiO_2$–4C and Ni–$TiO_2$–9C, the $n_{dl}$ values are almost similar and are far from ideal capacitive behavior. This clearly shows that the

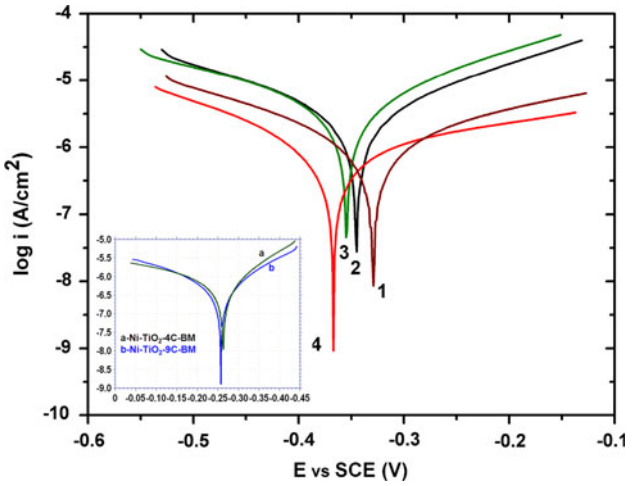


**Fig. 8** Tafel plots of electrodeposited *1* Ni, *2* Ni–$TiO_2$–4C, *3* Ni–$TiO_2$–9C, and *4* Ni–$TiO_2$–CM coatings and *inset* shows the Tafel plots of *a* Ni–$TiO_2$–4C–BM and *b* Ni–$TiO_2$–9C–BM electrodeposited from ball-milled powders

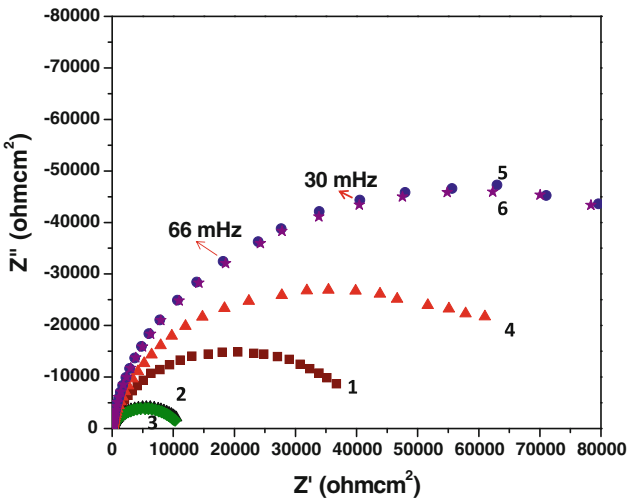


**Fig. 9** Nyquist plots of electrodeposited *1* Ni, *2* Ni–$TiO_2$–4C, *3* Ni–$TiO_2$–9C, *4* Ni–$TiO_2$–CM, *5* Ni–$TiO_2$–4C–BM, and *6* Ni–$TiO_2$–9C–BM coatings

**Table 1** Potentiodynamic polarization and electrochemical impedance data of Ni and Ni–$TiO_2$ composite coatings

| Sample | $i_{corr}$ (μA $cm^{-2}$) | $R_p$ (kΩ $cm^2$) | $R_s$ (Ω $cm^2$) | $Q_{dl} - Y_0$ (μS $s^n cm^{-1}$) | $n_{dl}$ | $R_{ct}$ (kΩ $cm^2$) |
|---|---|---|---|---|---|---|
| Ni | 0.85 | 34.25 | 1.11 | 40.0 | 0.923 | 35.17 |
| Ni–$TiO_2$–4C | 2.50 | 10.45 | 1.12 | 91.1 | 0.886 | 10.37 |
| Ni–$TiO_2$–4C–BM | 0.39 | 86.62 | 1.11 | 48.6 | 0.949 | 95.65 |
| Ni–$TiO_2$–9C | 2.98 | 10.10 | 1.05 | 98.9 | 0.875 | 9.930 |
| Ni–$TiO_2$–9C–BM | 0.49 | 70.67 | 1.37 | 51.2 | 0.939 | 100.00 |
| Ni–$TiO_2$–CM | 0.69 | 55.87 | 1.07 | 36.0 | 0.914 | 63.80 |

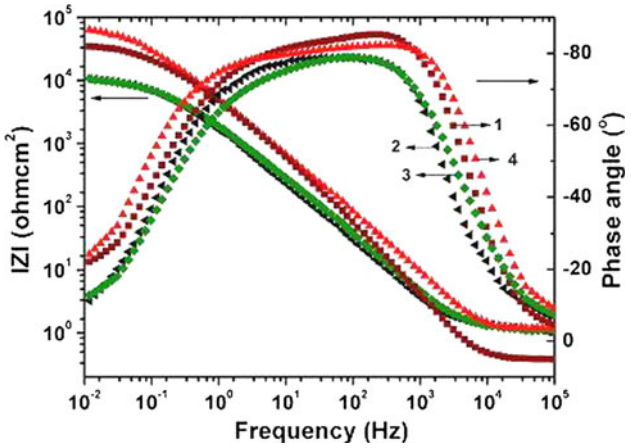


**Fig. 10** Bode plots of electrodeposited *1* Ni, *2* Ni–$TiO_2$–4C, *3* Ni–$TiO_2$–9C, and *4* Ni–$TiO_2$–CM coatings

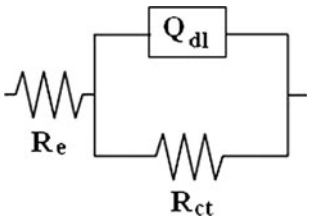


**Fig. 11** Equivalent circuit for Ni and Ni–$TiO_2$ composite coatings

surface in-homogeneities in these two coatings are higher with respect to composition and morphology. Also, the $R_{ct}$ values of these coatings are lower than plain Ni. This could be due to the higher surface roughness of the coatings (~0.7 and ~0.9 μm, respectively for Ni–$TiO_2$–4C and Ni–$TiO_2$–9C) compared to the surface roughness of Ni–$TiO_2$–CM (~0.45 μm) coating. This has been further substantiated by the fact that upon reducing the particle size of titania powders used in Ni–$TiO_2$–4C–BM and Ni–$TiO_2$–9C–BM coatings, the surface roughness of the coatings reduced to ~0.3 and ~0.4 μm, respectively and in turn the corrosion resistance improved with lowered $i_{corr}$ values. The uniform distribution of particles could have also resulted in uniform corrosion. The appropriate equivalent circuit used for fitting the parameters of Ni and Ni–$TiO_2$ coatings is shown in Fig. 11. The $R_{ct}$ and $Q_{dl}$ elements assigned in the equivalent circuit are related to the properties of the coating and electrolyte/coating interface reaction.

There have been a large number of deliberations on the effect of surface roughness on the corrosion resistance of the coatings. In general, the surface roughness plays a role on the corrosion behavior of metallic materials [26, 27]. It has been reported that an increase in the surface roughness of stainless steels increases the pitting susceptibility and general corrosion rate [28]. A similar trend has been reported for other metals, such as copper and titanium-based alloys. Here, is an example where in the effect of surface roughness on corrosion resistance of electrodeposited Ni–$TiO_2$ composite coatings is shown.

### 3.4 Tribological behavior of Ni–$TiO_2$ coatings

The wear data of Ni–$TiO_2$ composite coatings are tabulated in Table 2. It can be seen from table 2 that Ni–$TiO_2$–CM coating showed the lowest wear loss, followed by Ni–$TiO_2$–4C and Ni–$TiO_2$–9C coatings. The Ni–$TiO_2$–CM composite coating having large number of smaller anatase particles, exhibited lowest friction coefficient and wear rate. Despite the higher microhardness, Ni–$TiO_2$–9C exhibited poor wear resistance probably due to the poor adhesion of larger sized titania particles to the nickel matrix. In the case of Ni–$TiO_2$–CM coating very little material was transferred to the disk (Fig. 12). In case of Ni–$TiO_2$–4C transferred disk, there was a partial oxide film formation (Fig. 12a) and the same was absent in Ni–$TiO_2$–9C transferred disk (Fig. 12c). Due to the local heating and available oxygen, the oxide film formation could have taken place on the disk corresponding to the transfer of Ni–$TiO_2$–CM composite coating (Fig. 12e).

### 3.5 Wettability of as deposited and FAS-treated Ni and Ni–$TiO_2$ coatings

Surface wettability is of great importance to the performance of materials and coatings. It is well-known that surface wetting behavior is mainly dictated by surface chemical composition and morphology. The effect of current density on the structure and hydrophobicity of the coatings was studied by Huang and Pan [19]. They found that the WCA increased with increasing current density for FAS treated Ni–$TiO_2$ composite coatings. The WCA of as electrodeposited plain nickel and FAS-treated plain nickel coatings have not been reported. Similar trend was also observed in

**Table 2** Wear data of Ni–$TiO_2$ coatings

| Sample | Total height loss (μm) | Coefficient of friction | Wear volume ($mm^3$) |
|---|---|---|---|
| Ni–$TiO_2$–4C | 9 | 0.761 | 0.0015253 |
| Ni–$TiO_2$–9C | 40 | 0.538 | 0.03155 |
| Ni–$TiO_2$–CM | 6 | 0.363 | 0.000678 |

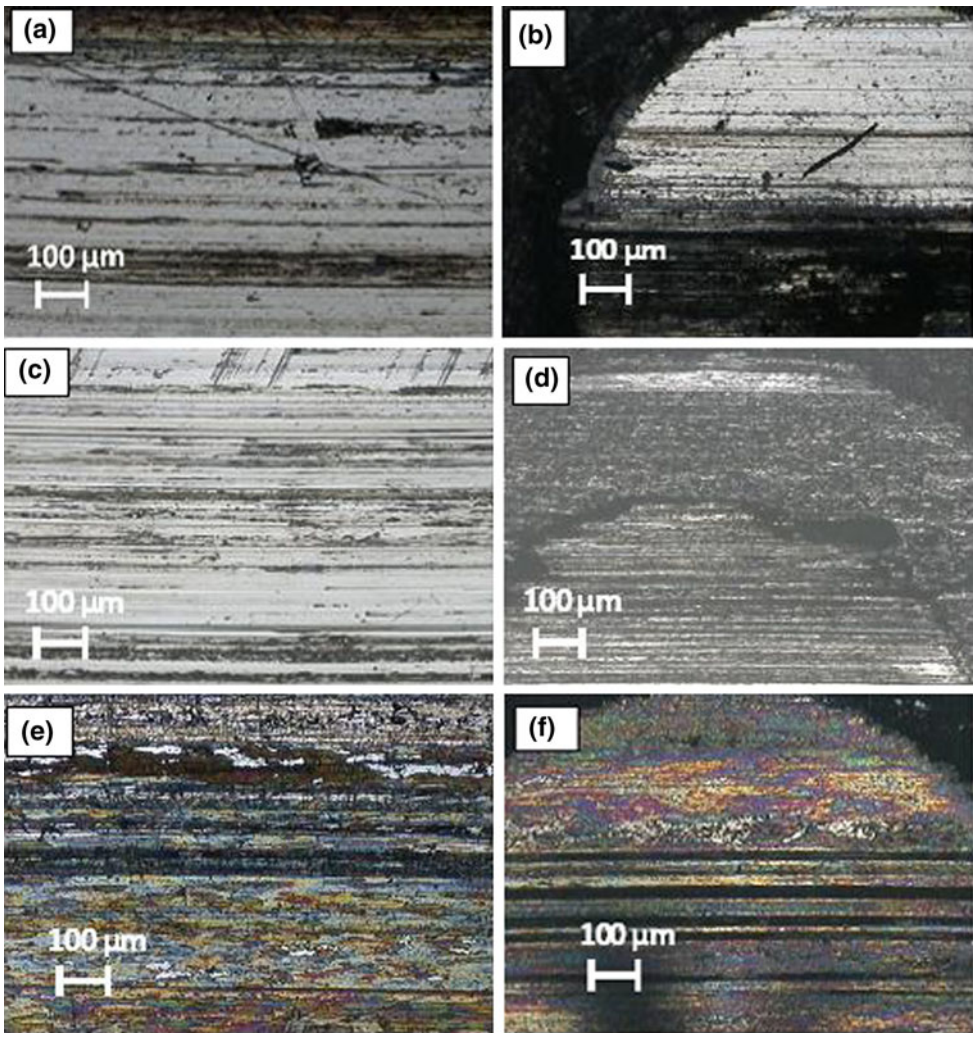


**Fig. 12** Optical micrographs of the wear tracks of the pins coated with **a** Ni–$TiO_2$–4C, **c** Ni–$TiO_2$–9C, **e** Ni–$TiO_2$–CM and **b**, **d**, and **f** are their corresponding wear tracks on disks

**Table 3** Water contact angles of FAS-treated Ni and Ni–$TiO_2$ composite coatings as a function of applied current density

| Current density (A $dm^{-2}$) | WCA of Ni (°) | | WCA of Ni–$TiO_2$–4C (°) | | WCA of Ni–$TiO_2$–9C (°) | | WCA of Ni–$TiO_2$–CM (°) | |
|---|---|---|---|---|---|---|---|---|
| | As-prepared | FAS treated | As-prepared | FAS treated | As-prepared | FAS treated | As-prepared | FAS treated |
| 0.77 | 83 | 107 | 121 | 148 | 50 | 154 | 49 | 150 |
| 1.55 | 89 | 109 | 130 | 129 | 56 | 157 | 50 | 153 |
| 3.1 | 93 | 110 | 142 | 144 | 103 | 157 | 35 | 153 |
| 5.4 | 104 | 108 | 141 | 156 | 81 | 151 | 63 | 137 |

the present study and the values have been tabulated in Table 3.

Among the coatings studied in the present investigation, Ni–$TiO_2$–9C exhibited the maximum WCA of 157°. The influence of current density on surface roughness of the coatings was studied and the plots are shown in Fig. 13. Higher surface roughness and highest WCA was exhibited by Ni–$TiO_2$–9C coating.

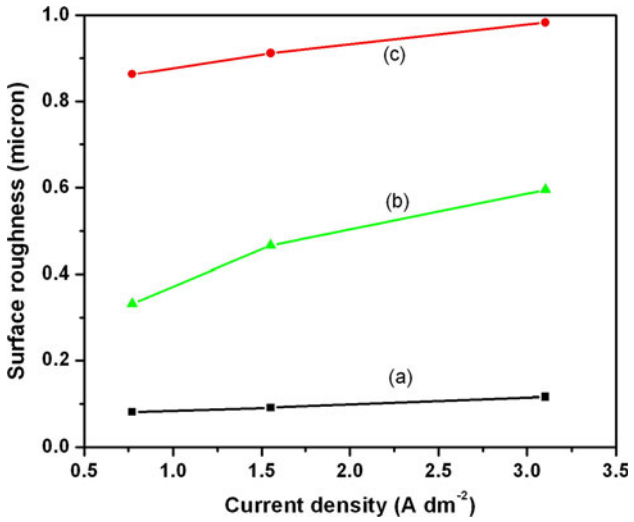


**Fig. 13** Plots of surface roughness vs. current density of FAS treated *a* Ni, *b* Ni–$TiO_2$–9C and *c* Ni–$TiO_2$–CM coatings

## 4 Conclusions

In the present work, the effect of the preparation of titania particles on the properties of electrodeposited Ni–$TiO_2$ coating was studied. This study has shown that the calcination temperature of the precipitation synthesized titania particles will determine the phase, size, and distribution of agglomerated particles. The sizes of the codeposited particles, in turn play an important role on the properties of the Ni-composite coatings. The Ni–$TiO_2$–CM coating having smaller sized agglomerates exhibited better corrosion and wear resistance compared to the Ni–$TiO_2$–4C and Ni–$TiO_2$–9C coatings containing larger agglomerates. However, the incorporation of $TiO_2$–4C and $TiO_2$–9C ball-milled particles enhanced the corrosion resistance. This study has shown that the size of codeposited particles and in turn, the surface roughness plays an important role in tailoring the corrosion resistance of the Ni-composite coatings. This study has also shown that it is possible to reduce the particle size of the precipitation synthesized titania particles such that it enhances the corrosion resistance of the nickel matrix that is equivalent to that of commercial titania particles. The higher surface roughness of Ni–$TiO_2$ coatings along with a surface treatment with a low surface energy material like fluoroalkyl silane imparted superhydrophobic property and among all these coatings, Ni–$TiO_2$–9C coating exhibited a maximum WCA of 157°.

**Acknowledgments** The authors thank Director, NAL for his constant encouragement. The authors acknowledge the financial assistance received from CSIR (Project No. SIP-SED-02). The authors also thank Mujibir, G. Savitha, A. Sreenivasan, Siju, Latha, Manikandanath, Jyothi and Dinesh for the help received in electrodeposition, corrosion testing, FESEM, microhardness, Raman spectroscopy and contact angle measurements. The authors also thank Mrs. R. V. Lakshmi for the help received in the fluoroalkyl surface treatment.

## References

1. Garcia I, Fransaer J, Celis J-P (2001) Electrodeposition and sliding wear resistance of nickel composite coatings containing micron and submicron SiC particles. Surf Coat Technol 148:171–178. doi:10.1016/S0257-8972(01)01336-6
2. Rickerby DS, Matthews A (1991) Advanced surface coatings: a handbook of surface engineering. Blackie, Glasgow
3. Rizzo M, Bruno G, Westerlund AG, Vartiainen J, Tepe B, Nomura K, Morent R (2009) Surface coatings. Nova Science Publishers, New York
4. Dennis JK, Such TE (1993) Nickel and chromium plating, 3rd edn. Woodhead Publishing, Cambridge
5. Temam HB, Chala A, Rahmane S (2011) Microhardness and corrosion behavior of Ni–SiC electrodeposited coatings in presence of organic additives. Surf Coat Technol 205:S161–S164. doi:10.1016/j.surfcoat.2011.04.086
6. Aruna ST, Bindu CN, Ezhil Selvi V, William Grips VK, Rajam KS (2006) Synthesis and properties of electrodeposited Ni/ceria nanocomposite coatings. Surf Coat Technol 200:6871–6880. doi:10.1016/j.surfcoat.2005.10.035
7. Li JM, Yin JY, Cai C, Zhang Z, Li JF, Yang JF, Xue MZ, Liu YG (2012) Corrosion behavior of nanostructured Ni–$Si_3N_4$ composite films: a study of electrochemical impedance spectroscopy. Mater Corros 63:622–626. doi:10.1002/maco.201005970
8. Wang W, Hou F-Y, Wang H, Guo H-T (2005) Fabrication and characterization of Ni–$ZrO_2$ composite nano-coatings by pulse electrodeposition. Scr Mater 53:613–618. doi:10.1016/j.scriptamat.2005.04.002
9. Guo C, Zuo Y, Zhao X, Zhao J, Xiong J (2008) The effects of electrodeposition current density on properties of Ni–CNTs composite coatings. Surf Coat Technol 202:3246–3250. doi:10.1016/j.surfcoat.2007.11.032
10. Tsubota T, Tanii S, Ishida T, Nagata M, Matsumoto Y (2005) Composite electroplating of Ni and surface-modified diamond particles with silane coupling reagent. Diam Relat Mater 14:608–612. doi:10.1016/j.diamond.2005.01.013
11. Li J, Sun Y, Sun X, Qiao J (2005) Mechanical and corrosion-resistance performance of electrodeposited titania–nickel nanocomposite coatings. Surf Coat Technol 192:331–335. doi:10.1016/j.surfcoat.2004.04.082
12. Yang X-K, Li Q, Hu J-Y, Zhong X-K, Zhang S-Y (2010) The electrochemical corrosion behavior of sealed Ni–$TiO_2$ composite coating for sintered NdFeB magnet. J Appl Electrochem 40:39–47. doi:10.1007/s10800-009-9961-8
13. Parida G, Chaira D, Chopkar M, Basu A (2011) Synthesis and characterization of Ni–$TiO_2$ composite coatings by electro-co-deposition. Surf Coat Technol 205:4871–4879. doi:10.1016/j.surfcoat.2011.04.102
14. Baghery P, Farzam M, Hosseini M (2010) Ni–$TiO_2$ nanocomposite coating with high resistance to corrosion and wear. Surf Coat Technol 204:3804–3810. doi:10.1016/j.surfcoat.2010.04.061
15. Sun XJ, Li JG (2008) Tribological characterization of electro-deposited nickel-titania nanocomposite coatings sliding against silicon nitride in high vacuum. Surf Eng 24:236–239. doi:10.1179/174329408X286060
16. Sun XJ, Li JG (2007) Friction and wear properties of electrodeposited nickel–titania nanocomposite coatings. Tribol Lett 28:223–228. doi:10.1007/s11249-007-9254-5

17. Lajevardi SA, Shahrabi T (2010) Effects of pulse electrodeposition parameters on the properties of Ni–$TiO_2$ nanocomposite coatings. Appl Surf Sci 256:6775–6781. doi:10.1016/j.apsusc.2010.04.088
18. Chen W, Gao W (2010) Sol-enhanced electroplating nanostructured Ni–$TiO_2$ composite coatings—the effects of sol concentration on the mechanical and corrosion properties. Electrochim Acta 55:6865–6871. doi:10.1016/j.electacta.2010.05.079
19. Huang S, Wei-Pan YH (2011) Relationship between the structure and hydrophobic performance of Ni–$TiO_2$ nanocomposite coatings by electrodeposition. Surf Coat Technol 205:3872–3876. doi:10.1016/j.surfcoat.2011.01.065
20. Wu YJ, Fu HP, Hong RY, Zheng Y, Wei DG (2009) Influence of surfactants on co-precipitation synthesis of Bi–YIG particles. J Alloys Compd 470:497–501. doi:10.1016/j.jallcom.2008.03.025
21. Aruna ST, William Grips VK, Rajam KS (2009) Ni-based electrodeposited composite coating exhibiting improved microhardness, corrosion and wear resistance properties. J Alloys Compd 468:546–552. doi:10.1016/j.jallcom.2008.01.058
22. Holm R (1946) Electric contacts. Almquist and Wiksells, Stockholm (Sect. 40)
23. Archard JF (1953) Contact and rubbing of flat surfaces. J Appl Phys 24:981–988. doi:10.1063/1.1721448
24. Wang C, Deng Z-X, Li Y (2001) The synthesis of nanocrystalline anatase and rutile titania in mixed organic media. Inorg Chem 40:5210–5214. doi:10.1021/ic0101679
25. Szczygiel B, Kolodziej M (2005) Composite Ni/$Al_2O_3$ coatings and their corrosion resistance. Electrochim Acta 50:4188–4195. doi:10.1016/j.electacta.2005.01.040
26. Honga T, Nagumo M (1997) Effect of surface roughness on early stages of pitting corrosion of Type 301 stainless steel. Corros Sci 39:1665–1672. doi:10.1016/S0010-938X(97)00072-3
27. Yoo B, Shin K-R, Hwang DY, Lee DH, Shin DY (2010) Effect of surface roughness on leakage current and corrosion resistance of oxide layer on AZ91Mg alloy prepared by plasma electrolytic oxidation. Appl Surf Sci 256:6667–6672. doi:10.1016/j.apsusc.2010.04.067
28. Shahryari A, Kamal W, Omanovic S (2008) The effect of surface roughness on the efficiency of the cyclic potentiodynamic passivation (CPP) method in the improvement of general and pitting corrosion resistance of 316LVM stainless steel. Mater Lett 62:3906–3909. doi:10.1016/j.matlet.2008.05.032